7. Burd DAR, Santis G, Milward TM. Severe extravasation injury: an avoidable introgenic disaster. *Br Med J.* 1985;290:1579–1580.
8. McAlister WH, Palmer K. The histologic effects of four commonly used media for excretory urography and an attempt to modify the response. *Radiology.* 1971;99:511–516.
9. Cohan RH, Leder RA, Bolick D, et al. Extravascular extravasation of radiographic contrast media: effects of conventional and low-osmolar agents in the rat thigh. *Invest Radiol.* 1990;25:504–510.
10. Kim SH, Park JH, Kim YI, et al. Experimental tissue damage after subcutaneous injection of water soluble contrast media. *Invest Radiol.* 1990;25:678–685.
11. McAlister WH, Kissane JM. Comparison of soft tissue effects of conventional ionic low osmolar ionic and nonionic iodine containing contrast material in experimental animals. *Pediatr Radiol.* 1990;20:170–174.
12. Spitany H, Koltz PF, Mays C, et al. CT contrast extravasation in the upper extremity: strategies for management. *Int J Surg.* 2010; 8:384–386.
13. Bellin MF, Jakobsen JA, Tomassin I, et al. Contrast medium extravasation injury: guidelines for prevention and management. *Eur Radiol.* 2002;12:2807–2812.
14. Paice T. Economic Impact of an Extravasation: An Analysis. *Imaging Economics.* 2007.
15. Nelson RC, Anderson FA Jr, Birnbaum BA, et al. Contrast media extravasation during dynamic CT: detection with an extravasation detection accessory. *Radiology.* 1998;209:837–843.
16. Birnbaum BA, Nelson RC, Chezmar JL, et al. Extravasation detection accessory: clinical evaluation in 500 patients. *Radiology.* 1999;212:431–438.
17. Bouton CE, Lombardi T, Hobson FR, et al. Experimental detection of subcutaneous contrast extravasation using radio frequency permittivity sensing. *J Comput Assist Tomogr.* 2009;33:824–7.
18. Ishihara T, Kobayashi T, Ikeno N, et al. Development of innovative contrast medium extravasation detection system for intravenous imaging CT examinations. *ECR.* 2010; Scientific exhibit 10-E-971-ECR.
19. Kashima S, Nishihara M, Kondo T, et al. Model for measurement of tissue oxygenated blood volume by the dynamic light scattering method. *Jpn J Appl Phys.* 1992;31:4097–4102.
20. Vegfors M, Lindberg LG, Oberg PA, et al. Accuracy of pulse oximetry at various haematocrits and during haemolysis in an in vitro model. *Med Biol Eng Comput.* 1993;31:135–141.
21. Sistrom CL, Gay SB, Peffly L. Extravasation of iopamidol and iohexol during contrast-enhanced CT: report of 28 cases. *Radiology.* 1991;180:707–710.
22. Tublin ME, Tessler FN, Cheng SL, et al. Effect of injection rate of contrast medium on pancreatic and hepatic helical CT. *Radiology.* 1999;210:97–101.
23. Kim T, Mrakami T, Takahashi S, et al. Pancreatic CT imaging: effects of different injection rates and doses of contrast material. *Radiology.* 1999;212:219–225.
24. Han JK, Choi BI, Kim AY, et al. Contrast media in abdominal computed tomography: optimization of delivery methods. *Korean J Radiol.* 2001;2:28–36.
25. Jacobs JE, Birbaum BA, Langlotz CP, et al. Contrast media reactions and extravasation: relationship to intravenous injection rates. *Radiology.* 1998;209:411–416.
26. Cohan RH, Bullard MA, Ellis JH, et al. Local reactions after injection of iodinated contrast material: detection, management, and outcome. *Acad Radiol.* 1997;4:711–718.
27. Harmon BH, Berland LL, Lee JY. Effect of varying rates of low-osmolarity contrast media injection for hepatic CT: correlation with iodocyanine green transit time. *Radiology.* 1992;184:379–382.
28. Kopka L, Rodenwaldt J, Fisher U, et al. Dual-phase helical CT of the liver. *Effects of bolus tracking and different volumes of contrast material. Radiology.* 1996;201:321–326.
29. Dinkel HP, Fieger M, Knupffer J, et al. Optimizing liver contrast in helical liver CT: value of a real-time bolus-tracking technique. *Eur Radial.* 1998;8:1608–1612.
30. Bae Kyongtae T. Test-bolus versus bolus-tracking techniques for CT angiographic timing. *Radiology.* 2005;236:369–370.

Available online at www.sciencedirect.com

ScienceDirect

journal homepage: www.JournalofSurgicalResearch.com

Pancreatic perfusion data and post-pancreaticoduodenectomy outcomes

Motokazu Sugimoto, MD, PhD,[a,b] *Shinichiro Takahashi, MD, PhD,*[a,*] *Tatsushi Kobayashi, MD,*[c] *Motohiro Kojima, MD, PhD,*[b] *Naoto Gotohda, MD, PhD,*[a] *Mitsuo Satake, MD,*[c] *Atsushi Ochiai, MD, PhD,*[b] *and Masaru Konishi, MD*[a]

[a] *Department of Hepatobiliary-Pancreatic Surgery, National Cancer Center Hospital East, Kashiwa, Chiba, Japan*
[b] *Division of Pathology, Research Center for Innovative Oncology, National Cancer Center Hospital East, Kashiwa, Chiba, Japan*
[c] *Department of Radiology, National Cancer Center Hospital East, Kashiwa, Chiba, Japan*

ARTICLE INFO

Article history:
Received 30 September 2014
Received in revised form
10 November 2014
Accepted 26 November 2014
Available online xxx

Keywords:
Pancreatic CT perfusion
Postoperative pancreatic fistula
Pancreaticoduodenectomy
Fibrosis

ABSTRACT

Background: Precise risk assessment for postoperative pancreatic fistula (POPF) after pancreaticoduodenectomy (PD) may be facilitated using imaging modalities. Computed tomography perfusion (CTP) of the pancreas may represent histologic findings. This study aimed to evaluate the utility of CTP data for the risk of POPF after PD, in relation to histologic findings.

Methods: Twenty patients who underwent preoperative pancreatic CTP measurement using 320-detector row CT before PD were investigated. Clinicopathologic findings, including CTP data, were analyzed to assess the occurrence of POPF. In addition, the correlation between CTP data and histologic findings was evaluated.

Results: POPF occurred in 11 cases (grade A, 6; grade B, 5; and grade C, 0). In CTP data, both high arterial flow (AF) and short mean transit time (MTT) were related to POPF occurrence ($P = 0.001$, $P = 0.001$). AF was negatively correlated with fibrosis in the pancreatic parenchyma ($r = -0.680$), whereas MTT was positively correlated with fibrosis ($r = 0.725$). AF >80 mL/min/100 mL and MTT <16 s showed high sensitivity, specificity, positive predictive value, and negative predictive value (80.0%, 100.0%, 100.0%, and 83.3%, respectively) for the occurrence of POPF.

Conclusions: CTP data for the pancreas were found to be correlated with the occurrence of POPF after PD. Alterations in the blood flow to the remnant pancreas may reflect histological changes, including fibrosis in the pancreatic stump, and influence the outcome after PD. CTP may thus facilitate objective and quantitative risk assessment of POPF after PD.

1. Introduction

Soft pancreatic consistency has traditionally been regarded as a definite risk factor for postoperative pancreatic fistula (POPF) after pancreaticoduodenectomy (PD); however, the consistency is assessed intraoperatively in a subjective and qualitative manner [1–3]. On the other hand, objective and quantitative assessment of POPF risk using preoperative imaging modalities, such as computed tomography (CT) or magnetic resonance imaging (MRI), have been increasingly reported [4–8].

* *Corresponding author.* Department of Hepatobiliary-Pancreatic Surgery, National Cancer Center Hospital East, 6-5-1 Kashiwa-no-ha, Kashiwa, Chiba 277 8577, Japan. Tel.: +81 4 7133 1111; fax: +81 4 7131 4724.
E-mail address: shtakaha@east.ncc.go.jp (S. Takahashi).
0022-4804/$ – see front matter © 2014 Elsevier Inc. All rights reserved.
http://dx.doi.org/10.1016/j.jss.2014.11.046

Computed tomography perfusion (CTP) is a functional imaging technique that is used to assess hemodynamic changes in an organ, and its utility in the diagnosis of cerebrovascular and coronary artery disease has been widely reported [9,10]. In 1995, Miles *et al.* [11] demonstrated the feasibility of absolute quantification to assess blood perfusion in the pancreas for the first time. Subsequently, circulatory alterations were reported in patients with acute or chronic pancreatitis [12–14]. A new generation of CT systems with 320-detector rows offers significant advantages over conventional multidetector CT. Using 320-detector row CT, volumetric acquisition over a range of 16 cm can be achieved with single-rotation scanning, with acceptable image quality and relatively low radiation exposure [15–18]. Therefore, this technique makes it possible to obtain perfusion data of the entire pancreas by performing only one dynamic volume scan with the administration of a single contrast material bolus.

A few studies have reported the clinical utility of CTP of the pancreas using 320-detector row CT. Kandel *et al.* [15] have stated that the perfusion of pancreatic carcinomas is significantly lower than that of normal pancreatic tissue. In hepatic CTP imaging, parameters obtained using CTP have been reported to be correlated with fibrotic changes in liver biopsy specimens [19,20]. Therefore, CTP data may reflect the histologic findings for the specific organ. However, to our knowledge, no such comparison of CTP data with histologic findings has been reported for the pancreas. The aims of the present study were to evaluate the correlations between preoperative CTP data and the incidence of POPF after PD as well as with histologic findings.

2. Material and methods

2.1. Patients and clinical data collection

Between March 2012 and February 2013, 20 patients who were scheduled to undergo PD were prospectively recruited for preoperative CTP examination at the National Cancer Center Hospital East, Japan. All patients were examined by preoperative contrast-enhanced multidetector row CT focusing on the lesion, as part of the diagnostic workup; subsequently, PD was indicated for suspected malignancy. CTP was then performed in patients from whom written consent was obtained. Clinicopathologic data were reviewed from medical records. This study was approved by the Institutional Review Board of the National Cancer Center.

2.2. Surgical techniques and preoperative management

Details of the surgical maneuvers and preoperative management have been mentioned in our previous article [21]. Subtotal stomach-preserving PD [22] and modified Child reconstruction were performed in all cases. End-to-side pancreaticojejunostomy with the placement of a 6Fr internal short stent through the main pancreatic duct (MPD) was performed as a two-layered anastomosis using interrupted duct-to-mucosa sutures, with coverage of the entire cut surface of the pancreas by the seromuscular layer of the jejunum. Pancreatic consistency was evaluated subjectively as soft or hard by the surgeon during the operation. The definition of POPF was based on the classification of the International Study Group on Pancreatic Fistula [23].

2.3. Acquisition and interpretation of CTP data

Patients were examined using a 320-detector row CT (Aquilion ONE; Toshiba Medical Systems Corporation, Ohtawara, Japan). Slices for CTP were selected from precontrast abdominopelvic helical scans and included images as large as an entire pancreas. For CTP, 60 mL of a nonionic contrast material (Iohexol, Ioverin 350; Teva Pharma Japan Inc, Nagoya, Japan) was administered at a rate of 3.5 mL/s with a power injector (Dual Shot GX; Nemoto Kyorindo, Tokyo, Japan), followed by a 40-mL saline bolus. All dynamic CTP images were acquired with the following parameters: 0.5 mm slice thickness, 320 slices, 512 × 512 matrix, 100 kV, 60 mA, and 0.5 s gantry rotation time. The scans were performed 23 times during 6–180 s after injection of the contrast material under quiet breathing. The effective radiation dose for this protocol was 9.72 mSv. Misregistrations due to respiration and automatism were compensated automatically by the Body Registration software (Toshiba Medical Systems) on the console. Regions of interest (ROIs) were placed on the abdominal aorta at the level of the celiac axis, liver, and pancreas to generate time-density curves. Three different ROIs were then placed in the remnant pancreas (body and tail) on both axial and coronal CTP slices, and arterial flow (AF) (mL/min/100 mL) and mean transit time (MTT) (s) were measured at each ROI using the compartment model [24,25] using the Body Perfusion software (Toshiba Medical Systems). ROIs in the pancreas were made as large as possible while avoiding large vessels. Intermediate values for AF and MTT using the median of three ROIs in the axial and coronal slices were analyzed as the CTP data. Examples of two representative cases are shown in Figure 1A–D,E–H. All radiological analyses were performed by an experienced radiologist (T.K.), who was blinded to the operative outcomes and other clinicopathologic findings.

2.4. Histologic evaluation

Histological evaluation was performed as described in our previous article [26]. Formalin-fixed, paraffin-embedded specimens obtained from a pancreatic stump were cut into 3-μm thick serial sections. The sections were stained with hematoxylin and eosin (HE) to assess the area of the entire cut surface and MPD; azan-Mallory (azan) stain, to assess the degree of fibrosis; and anti-CD31 antibodies, to assess vessel number and density. Anti-CD31 immunohistochemical staining was performed automatically using a Ventana BenchMark ULTRA (Ventana Medical Systems, Tucson, AZ). Monoclonal anti-human CD31 antibody (Dako, Glostrup, Denmark) was used at a dilution of 1:200, and the conditions for antigen retrieval and primary antibody incubation were set at 95°C for 8 min and 35°C for 60 min, respectively. The slides were photographed using a NanoZoomer Digital Pathology virtual slide viewer (Hamamatsu Photonics, Hamamatsu, Japan) and subjected to morphometric analysis. Histologic analysis of the two cases for which CTP images are presented in Figure 1 A–D,E–H are shown in Figures 2 and 3. Morphometric analysis was performed as described in our previous article [26], and the details of the procedure are outlined in the

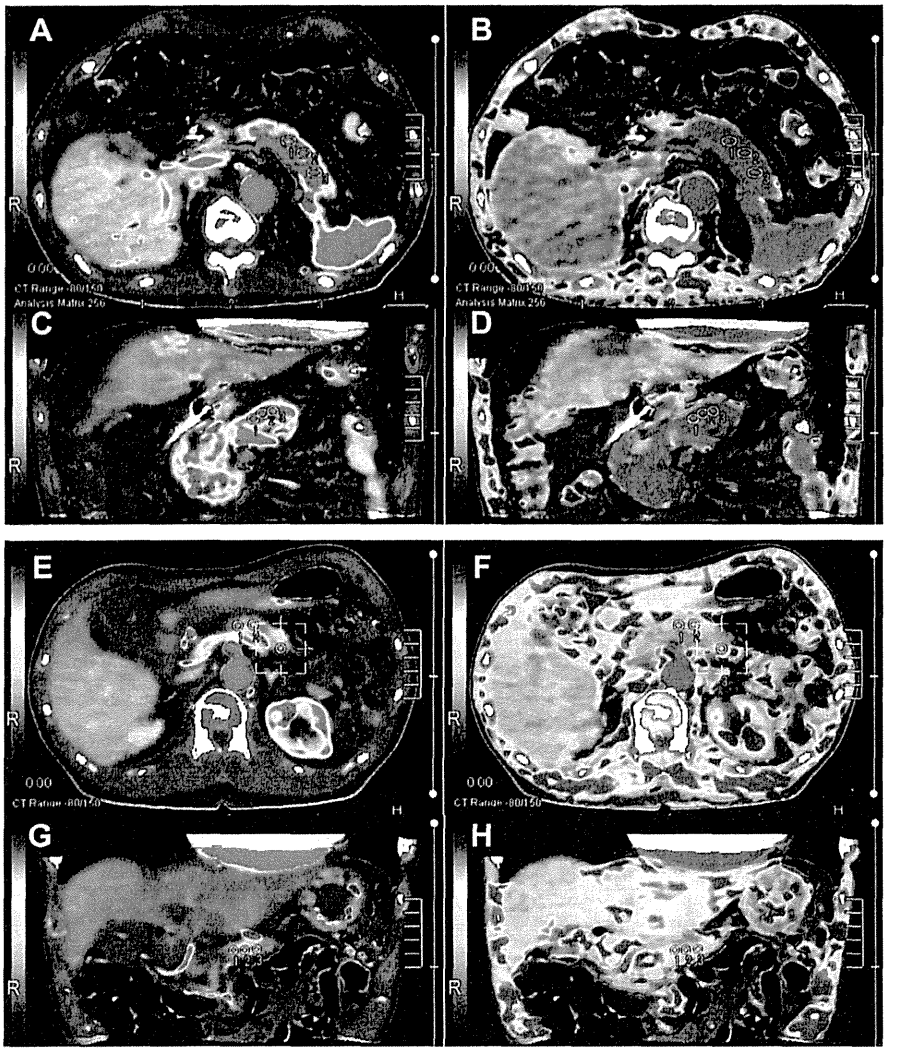

Fig. 1 – (A–D). Acquisition of CTP data for the remnant pancreas in Case 1; a 71-y-old male whose pancreas was intraoperatively palpated as soft, underwent PD for bile duct cancer and developed grade B POPF. CTP images: AF of axial slice (A), MTT of axial slice (B), AF of coronal slice (C), and MTT of coronal slice (D). Three different ROIs were placed in the remnant pancreas (body and tail) on the axial and coronal slices of CTP image. Average data for AF and MTT between the median of the three ROIs in the axial and coronal slices were 110.1 mL/min/100 mL and 9.0 s, respectively. (E–H). Acquisition of CTP data for the remnant pancreas in Case 2; a 70-y-old male with a hard pancreas who underwent PD for pancreatic adenocarcinoma and had an uneventful postoperative course. CTP images: AF of axial slice (E), MTT of axial slice (F), AF of coronal slice (G), and MTT of coronal slice (H). Average data for AF and MTT between the median of the three ROIs in the axial and coronal slices were 37.1 mL/min/100 mL and 43.0 s, respectively. (Color version of figure is available online.)

legends of Figures 2 and 3 in this article. One investigator (M.Su.) carried out all the histologic analyses under the supervision of an experienced pathologist (M.Koji.).

2.5. *Statistical analysis*

Univariate analysis was performed to compare preoperative patient characteristics, CTP data, pancreatic consistency, and histologic findings in the pancreatic stump between patients who did and did not develop POPF (grade A, B, or C). Categorical variables are summarized as numbers and percentages and were evaluated using chi-square test, whereas continuous variables are presented as median ± standard deviation and were evaluated using Mann–Whitney *U* test. Correlations between CTP data and clinicopathologic findings were evaluated using Spearman correlation coefficient *r*. All P values were based on two-sided statistical tests; the significance level was set at 0.05. All statistical analyses were performed using SPSS Statistics software (version 19.0; SPSS, Chicago, IL).

3. Results

3.1. *Relationship between clinicopathologic factors and POPF*

PD was performed for eight patients with pancreatic adenocarcinoma, three patients with bile duct cancer, three patients

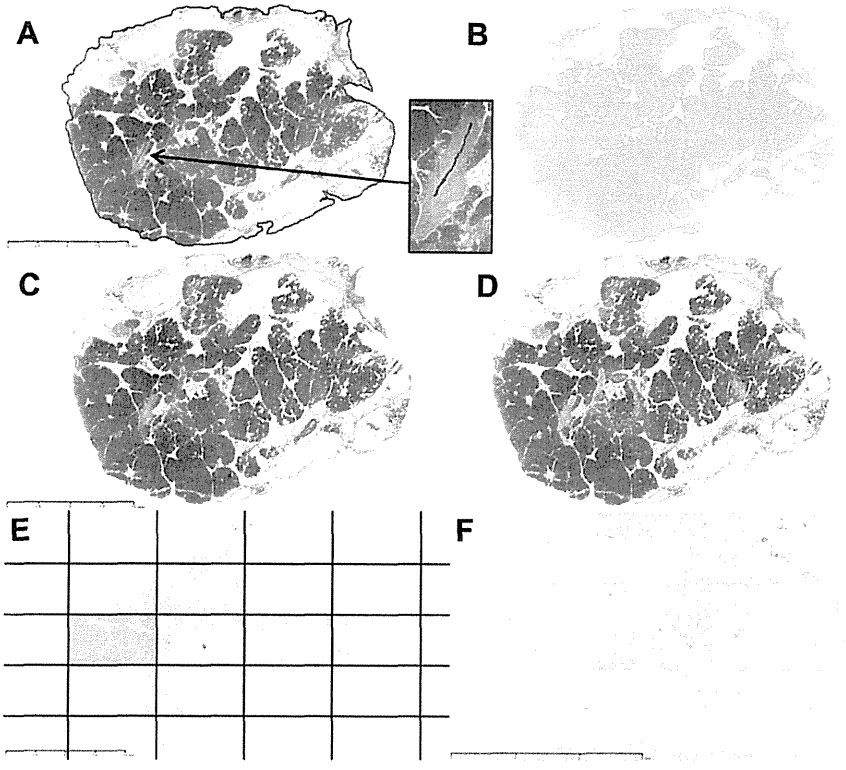

Fig. 2 – Histologic evaluation of the pancreatic stump in Case 1. (A) Loupe image of a HE-stained slide. The arrow indicates a magnified view of the MPD. The outer circumference of the entire cut surface (red line) and the inner circumference of the MPD lumen (blue line) were automatically outlined, and these areas were calculated using the tracing algorithm of the WinROOF software (version 6.5; Mitani Corporation, Tokyo, Japan). The area of the entire cut surface (within the red line) was 411.1 mm^2 and the MPD area (within the blue line) was 0.012 mm^2. The MPD ratio was 0.003%, calculated as the percentage area of MPD in the entire cut surface. (B) The HE-positive area was determined as the visualized area stained with HE using the color-detecting algorithm of the software and identified as bright green in this image. The area of fat was defined as the area of the entire cut surface minus the MPD area and the HE-positive area. The fat ratio was 36.3%, calculated as the percentage area of fat in the entire cut surface. (C) Azan-Mallory (azan) staining was evaluated on the loupe image to determine the degree of fibrosis. (D) The fibrosis area was defined as the visualized area stained with aniline blue using the color-detecting algorithm of the software and identified as bright green in this image. The fibrosis ratio was 2.4%, calculated as the percentage area of fibrosis in the entire cut surface. The lobular area was defined as the HE-positive area minus the MPD area and the fibrosis area. The lobular ratio was 61.3%, calculated as the percentage area of lobules in the entire cut surface. (E) Loupe image of immunohistochemical staining for CD31. The field was divided to allow separate evaluation on the magnified image. (F) Immunohistochemical staining for CD31 at ×4.0 magnification in the blue square shown in Figure 3E. The number of vessels was counted in terms of the number of CD31-immunopositive luminal structures visible in each field. The total number of vessels in the entire cut surface was 666, and the vessel density was 1.6/mm^2. (Color version of figure is available online.)

with ampullary cancer, two patients with intraductal papillary mucinous neoplasm, one patient with duodenal cancer, one patient with neuroendocrine tumor, one patient with solid pseudopapillary tumor, and one patient with autoimmune pancreatitis.

POPF occurred in 11 of the 20 patients (International Study Group on Pancreatic Fistula grade A in 6; grade B in 5; and grade C in 0). Table 1 shows the relationship between clinicopathologic factors and the occurrence of POPF. As compared with patients who did not develop POPF, patients who developed POPF showed a higher AF and shorter MTT in the CTP profile, a lower MPD ratio, lower fat ratio, lower fibrosis ratio, higher lobular ratio, and lower vessel density in the histologic assessment of the pancreatic stump. Figure 4 shows a scattergram of the CTP data and outcomes of POPF. A strong negative correlation was observed between AF and MTT ($r = -0.983$).

3.2. *Correlation between clinicopathologic factors and CTP data*

As shown in Table 2, AF was positively correlated with a soft pancreatic consistency, lobular ratio, and area of the entire cut surface, and negatively correlated with the presence of pancreatic adenocarcinoma, MPD ratio, fibrosis ratio, and vessel density. MTT was positively correlated with MPD ratio, fibrosis ratio, vessel density, and negatively correlated with a soft pancreatic consistency, lobular ratio, and area of the

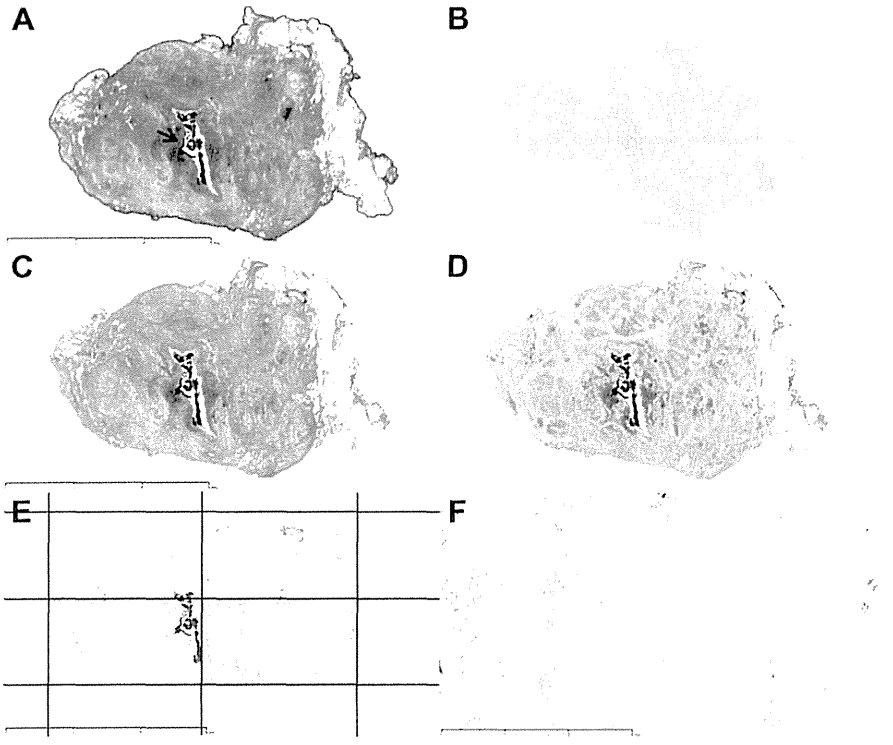

Fig. 3 – Histologic evaluation of the pancreatic stump in Case 2. (A) Loupe image of a HE-stained slide. Arrow indicates the MPD. The area of the entire cut surface (within the red line) was 101.7 mm^2, and the MPD area (within blue line) was 1.091 mm^2. The MPD ratio was 1.073%. (B) The fat ratio was 15.4%. (C) Azan-Mallory-stained slide in the loupe image. (D) The fibrosis ratio was 33.7%. The lobular ratio was 50.6%. (E) Loupe image of immunohistochemical staining for CD31. (F) Immunohistochemical staining for CD31 at ×4.0 magnification in the blue square shown in Figure 5E. The vessel density was 6.0/mm^2. (Color version of figure is available online.)

entire cut surface. Among the histologic features of the pancreatic stump, the fibrosis ratio was most strongly correlated with both AF and MTT ($r = -0.680$ and $r = 0.725$, respectively). POPF occurrence and the correlation between CTP data and the fibrosis ratio are shown in Figure 5. Moreover, a higher fibrosis ratio was correlated with a harder pancreatic consistency ($r = 0.609$), higher MPD ratio ($r = 0.686$), lower lobular ratio ($r = 0.690$), higher vessel density

Table 1 – Risk factor analysis for POPF after PD.

Variable	POPF ($n = 11$)	No POPF ($n = 9$)	P
Age	66 (27–82)	73 (50–80)	0.137
Sex (male %)	8 (72.7)	6 (66.7)	0.769
BMI (kg/m^2)	21.9 (20.3–30.5)	21.2 (18.3–27.6)	0.342
Diabetes, %	2 (18.2)	2 (22.2)	0.822
Pancreatic adenocarcinoma, %	3 (27.3)	5 (55.6)	0.199
CTP data			
AF (mL/min/100 mL)	107.0 (51.3–136.9)	37.1 (25.3–76.4)	0.001*
MTT (sec)	12.4 (7.9–24.0)	43.0 (16.9–63.1)	0.001*
Soft pancreatic consistency, %	9 (81.8)	4 (44.4)	0.081
Histological data			
MPD ratio (%)	0.102 (0.003–1.509)	0.578 (0.038–2.316)	0.030*
Fat ratio (%)	11.5 (7.2–36.3)	25.2 (12.2–44.4)	0.037*
Fibrosis ratio (%)	3.0 (1.1–11.3)	13.8 (2.5–33.7)	0.009*
Acinar gland ratio (%)	85.5 (61.3–89.3)	62.2 (30.4–85.3)	0.007*
Vessel density (mm^2)	1.1 (0.5–2.7)	2.1 (0.9–6.0)	0.017*
Area of entire cut surface (mm^2)	286.0 (157.9–557.4)	205.9 (101.7–374.3)	0.074

BMI = body mass index.
* $P < 0.05$. Differences between the two groups were evaluated using Mann–Whitney U test or chi-square test.

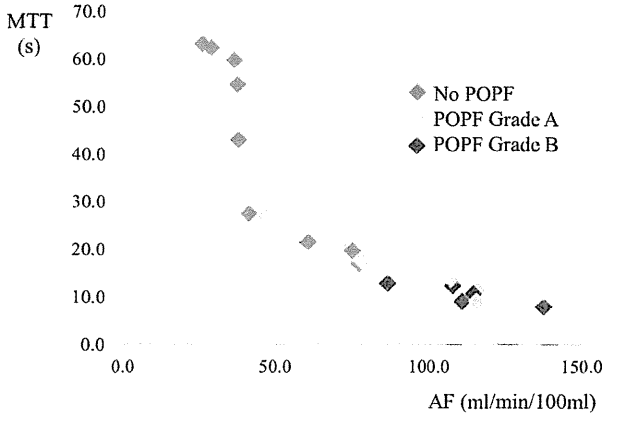

Fig. 4 – Relationship between CTP data for the remnant pancreas and occurrence of POPF after PD. (Color version of figure is available online.)

(r = 0.832), and smaller area of the entire cut surface (r = 0.504).

3.3. *Cutoff value of CTP data for the occurrence of POPF after PD*

Because the CTP data were strongly related to the occurrence of POPF after PD, the cutoff values of AF and MTT were determined using the receiver operating characteristic curve to assess their relationship with POPF. The areas under the receiver operating characteristic curve for the relationship between AF and POPF and between MTT and POPF were 0.949 and 0.939, respectively. When 80 mL/min/100 mL was set as the cutoff value for AF and 16 s as the cutoff value for MTT, the relevant cases were found to be identical. Sensitivity, specificity, positive predictive value, and negative predictive value of AF >80 mL/min/100 mL and MTT <16 s for the occurrence of POPF were 80.0%, 100.0%, 100.0%, and 83.3%, respectively.

Table 2 – Correlation between clinicopathologic factors and CTP data.

Variable	AF	MTT
Age	−0.127	0.140
Sex (male)	−0.265	0.189
BMI	0.015	−0.038
Diabetes	−0.325	0.303
Pancreatic adenocarcinoma	−0.460*	0.442
Soft pancreatic consistency	0.554*	−0.609**
MPD ratio	−0.650**	0.698**
Fat ratio	−0.289	0.250
Fibrosis ratio	−0.680**	0.725**
Lobular ratio	0.484*	−0.465*
Vessel density	−0.570**	0.589**
Area of the entire cut surface	0.484*	−0.552*

BMI = body mass index.
Significant correlations are indicated (*$P < 0.05$, **$P < 0.01$). Correlations between CTP data and clinicopathologic factors were evaluated using Spearman correlation coefficient r.

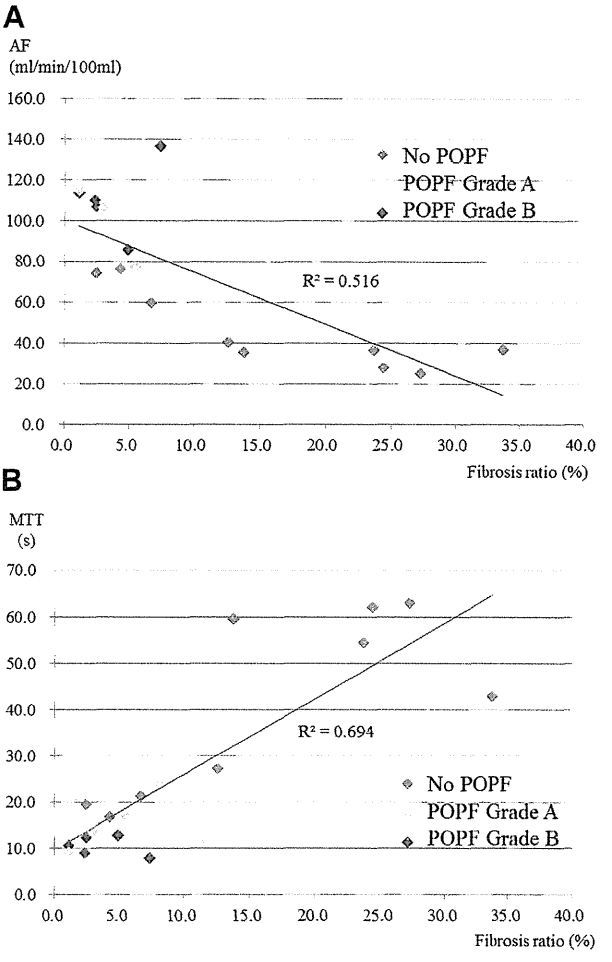

Fig. 5 – (A) POPF occurrence and correlation between AF and fibrosis ratio. (B) POPF occurrence and correlation between MTT and fibrosis ratio. (Color version of figure is available online.)

4. Discussion

In the present study, a high proportion of patients with high AF and short MTT of CTP developed POPF. Both high AF and short MTT were correlated with a soft pancreatic consistency and histologic features such as a lower MPD ratio, lower fibrosis ratio, higher lobular ratio, lower vessel density, and larger area of the entire cut surface. To the best of our knowledge, this is the first study to demonstrate the relationship between CTP data and POPF after PD and the correlation between CTP data and histologic findings. In this study, CTP data acquisition was homogenous and standardized, and the 320-detector row CT made it possible to acquire volumetric CTP data at multiple locations in multiple slices through the entire pancreas. Moreover, histologic evaluation was performed by computer-based automatic analysis. As the utility of morphometric image analysis for immunohistochemical specimens has increasingly been reported [26–29], we were able to estimate the correlation between radiographic and histologic findings in an objective and quantitative manner. This approach may extend our understanding of the

principles involved in the radiological depiction of hemodynamic alterations in the pancreas.

Among other options for predicting POPF after PD involving imaging modalities, the evaluation of the remnant pancreatic volume by preoperative CT or MRI [4], ratio of the pancreatic attenuation value between the hepatic and pancreatic phases as calculated by dual-phase CT [5], time-signal intensity curve of the pancreas obtained from dynamic contrast-enhanced MRI [6,7], and the ratio of signal intensity between the early arterial and portal-venous phases as evaluated by dynamic MRI [8] have been reported to be accurate predictors of POPF after PD. In a dynamic MRI study performed by Tajima *et al.* [7], the time-signal intensity curve profile was correlated with fibrosis of the pancreas, and a relationship between fibrosis and MPD dilation was suggested. In a study of pancreatic CT enhancement patterns, Hashimoto *et al.* [5] demonstrated that the risk of POPF was low in an atrophic, fibrotic pancreas. Likewise, CTP data may be able to predict POPF after PD accurately, as these data reflect histologic changes in the remnant pancreas. In a study of hepatic CTP, Ronot *et al.* [19] noted that MTT was an accurate parameter for differentiating the stages of fibrosis in patients with chronic hepatitis C virus infection.

In the present study, both low AF and prolonged MTT were strongly correlated with increased pancreatic fibrosis. Increased fibrosis was also correlated with a decreased number of pancreatic lobules, increased vessel density, a larger MPD lumen, and a smaller entire cut surface. Marked fibrosis in the pancreas might cause inflow disturbance and prolonged circulation within the organ. Interestingly, low AF was not correlated with decreased vessel density; rather, it showed a correlation with increased vessel density. Increased vessel density might be suggestive of increased neovascularity. Neovascularized microvessels do not contribute to effective blood flow in the organ, and therefore, cause a lower AF and prolonged MTT in such pancreas. Neovascularization, increased fibrosis, decreased lobules, a dilated MPD, and a small amount of pancreatic parenchyma indicate progressive morphologic alterations of the pancreatic parenchyma, consistent with chronic inflammation [26,30–32]. The relationship between these histologic changes and POPF are consistent with the results observed in a previous study by Friess *et al.* [33], who showed that the risk of POPF was low in pancreas with increased fibrosis and decreased exocrine function because of chronic pancreatitis. Therefore, the present study demonstrated that CTP parameters such as low AF and prolonged MTT reflect the progression of fibrosis in the pancreas and are suggestive of a lower risk of POPF.

In a clinical situation, CTP data—as an objective and quantitative parameter—may facilitate more definitive assessment of the risk of POPF after PD, and may allow meaningful comparisons among different institutions and studies, rather than intraoperatively assessed subjective pancreatic consistency. Using preoperative assessment with CTP data, the intraoperative procedures and/or perioperative management can be used as countermeasures for high-risk patients to reduce the incidence of POPF after PD. Recent meta-analyses have reported that reconstruction by pancreaticogastrostomy decreases the rate of POPF after PD in comparison with pancreaticojejunostomy [34,35]. In a recent randomized controlled study, the perioperative use of pasireotide, a somatostatin analog that has a longer half-life than octreotide and a broader binding profile, could reduce the risk and severity of POPF after PD [36]. Precise assessment of POPF risk may thus allow the use of these countermeasures, particularly for high-risk patients.

One of the limitations of this study is the relatively small number of patients included. The cutoff values of AF >80 mL/min/100 mL and MTT <16 s showed a strong relationship to the occurrence of POPF; however, the prognostic impact of CTP data for POPF can be evaluated only after examining data from a large number of patients. Moreover, the CTP data were only assessed using a compartment model for determination of MTT and AF. Comparison with other methods of CTP measurement might be necessary for accurate assessment. Furthermore, although preoperative CTP data were measured in sampled ROIs in the estimated remnant pancreas (body and tail), histologic examination was performed using specimens of the pancreatic cut edge. We assumed that the histologic findings of the pancreatic cut edge might represent the condition of the remnant pancreas.

5. Conclusions

In this preliminary study, high AF and low MTT were related to a high incidence of POPF after PD. These CTP data reflected characteristic histologic features in the pancreas, including low fibrosis, abundant pancreatic lobules, low vessel density, small MPD, and a large area of the entire cut surface, indicating a less-marked effect of chronic inflammation. Therefore, CTP data may enable preoperative, objective, and quantitative assessment of the risk of POPF after PD and allow surgeons to choose appropriate countermeasures against POPF.

Acknowledgment

The authors express special thanks to So Tsushima of the Application Development Group and Shinsuke Tsukagoshi of the CT Systems Development Department of Toshiba Medical Systems Corporation for their technical assistance with 320-detector row perfusion CT. This work was supported in part by Health and Labor Sciences Research grants for Third-term Comprehensive Control Research for Cancer (General-025) and Health and Labor Sciences Research grants for Research on Applying Health Technology.

Authors' contributions: M.Su. had full access to all the data and takes responsibility for data integrity and accuracy of the data analysis. M.Su., S.T., T.K., and M.Koni. contributed to the study concept and design. M.Su., S.T., T.K., M.Koji., N.G., and M.Koni. did the acquisition of data. M.Su., S.T., T.K., and M.Koji. did the analysis and interpretation of data and provided the administrative, technical, and material support. M.Su., T.K., and M.Koji. did the drafting of the article. M.Su., S.T., T.K., M.Koji., A.O., M.Sa., and M.Koni. did the critical revision of the article for important intellectual content.

M.Su., S.T., and T.K. did the statistical analysis. A.O., M.Sa., and M.Koni. did the study supervision.

Disclosure

The authors reported no proprietary or commercial interest in any product mentioned or concept discussed in the article.

REFERENCES

[1] Kawai M, Kondo S, Yamaue H, et al. Predictive risk factors for clinically relevant pancreatic fistula analyzed in 1,239 patients with pancreaticoduodenectomy: multicenter data collection as a project study of pancreatic surgery by the Japanese Society of Hepato-Biliary-Pancreatic Surgery. J Hepatobiliary Pancreat Sci 2011;18:601.

[2] Callery MP, Pratt WB, Kent TS, et al. A prospectively validated clinical risk score accurately predicts pancreatic fistula after pancreatoduodenectomy. J Am Coll Surg 2013;216:1.

[3] Lin JW, Cameron JL, Yeo CJ, et al. Risk factors and outcomes in postpancreaticoduodenectomy pancreaticocutaneous fistula. J Gastrointest Surg 2004;8:951.

[4] Frozanpor F, Loizou L, Ansorge C, et al. Preoperative pancreas CT/MRI characteristics predict fistula rate after pancreaticoduodenectomy. World J Surg 2012;36:1858.

[5] Hashimoto Y, Sclabas GM, Takahashi N, et al. Dual-phase computed tomography for assessment of pancreatic fibrosis and anastomotic failure risk following pancreatoduodenectomy. J Gastrointest Surg 2011;15:2193.

[6] Tajima Y, Kuroki T, Tsutsumi R, et al. Risk factors for pancreatic anastomotic leakage: the significance of preoperative dynamic magnetic resonance imaging of the pancreas as a predictor of leakage. J Am Coll Surg 2006;202:723.

[7] Tajima Y, Matsuzaki S, Furui J, et al. Use of the time-signal intensity curve from dynamic magnetic resonance imaging to evaluate remnant pancreatic fibrosis after pancreaticojejunostomy in patients undergoing pancreaticoduodenectomy. Br J Surg 2004;91:595.

[8] Dinter DJ, Aramin N, Weiss C, et al. Prediction of anastomotic leakage after pancreatic head resections by dynamic magnetic resonance imaging (dMRI). J Gastrointest Surg 2009; 13:735.

[9] Shinohara Y, Ibaraki M, Ohmura T, et al. Whole-brain perfusion measurement using 320-detector row computed tomography in patients with cerebrovascular steno-occlusive disease: comparison with 15O-positron emission tomography. J Comput Assist Tomogr 2010;34:830.

[10] Nasis A, Ko BS, Leung MC, et al. Diagnostic accuracy of combined coronary angiography and adenosine stress myocardial perfusion imaging using 320-detector computed tomography: pilot study. Eur Radiol 2013;23:1812.

[11] Miles KA, Hayball MP, Dixon AK. Measurement of human pancreatic perfusion using dynamic computed tomography with perfusion imaging. Br J Radiol 1995;68:471.

[12] Bize PE, Platon A, Becker CD, et al. Perfusion measurement in acute pancreatitis using dynamic perfusion MDCT. Am J Roentgenol 2006;186:114.

[13] Tsuji Y, Yamamoto H, Yazumi S, et al. Perfusion computerized tomography can predict pancreatic necrosis in early stages of severe acute pancreatitis. Clin Gastroenterol Hepatol 2007;5:1484.

[14] Arikawa S, Uchida M, Kunou Y, et al. Assessment of chronic pancreatitis: use of whole pancreas perfusion with 256-slice computed tomography. Pancreas 2012;41:530.

[15] Kandel S, Kloeters C, Meyer H, et al. Whole-organ perfusion of the pancreas using dynamic volume CT in patients with primary pancreas carcinoma: acquisition technique, post-processing and initial results. Eur Radiol 2009;19:2641.

[16] Goshima S, Kanematsu M, Nishibori H, et al. CT of the pancreas: comparison of anatomic structure depiction, image quality, and radiation exposure between 320-detector volumetric images and 64-detector helical images. Radiology 2011;260:139.

[17] Kanda T, Yoshikawa T, Ohno Y, et al. Perfusion measurement of the whole upper abdomen of patients with and without liver diseases: initial experience with 320-detector row CT. Eur J Radiol 2012;81:2470.

[18] Motosugi U, Ichikawa T, Sou H, et al. Multi-organ perfusion CT in the abdomen using a 320-detector row CT scanner: preliminary results of perfusion changes in the liver, spleen, and pancreas of cirrhotic patients. Eur J Radiol 2012;81:2533.

[19] Ronot M, Asselah T, Paradis V, et al. Liver fibrosis in chronic hepatitis C virus infection: differentiating minimal from intermediate fibrosis with perfusion CT. Radiology 2010; 256:135.

[20] Hashimoto K, Murakami T, Dono K, et al. Assessment of the severity of liver disease and fibrotic change: the usefulness of hepatic CT perfusion imaging. Oncol Rep 2006;16:677.

[21] Sugimoto M, Takahashi S, Gotohda N, et al. Schematic pancreatic configuration: a risk assessment for postoperative pancreatic fistula after pancreaticoduodenectomy. J Gastrointest Surg 2013;17:1744.

[22] Hayashibe A, Kameyama M, Shinbo M, et al. The surgical procedure and clinical results of subtotal stomach preserving pancreaticoduodenectomy (SSPPD) in comparison with pylorus preserving pancreaticoduodenectomy (PPPD). J Surg Oncol 2007;95:106.

[23] Bassi C, Dervenis C, Butturini G, et al. International Study Group on Pancreatic Fistula Definition. Postoperative pancreatic fistula: an international study group (ISGPF) definition. Surgery 2005;138:8.

[24] Ziegler SI, Haberkorn U, Byrne H, et al. Measurement of liver blood flow using oxygen-15 labelled water and dynamic positron emission tomography: limitations of model description. Eur J Nucl Med 1996;23:169.

[25] Materne R, Van Beers BE, Smith AM, et al. Non-invasive quantification of liver perfusion with dynamic computed tomography and a dual-input one-compartmental model. Clin Sci 2000;99:517.

[26] Sugimoto M, Takahashi S, Kojima M, et al. What is the nature of pancreatic consistency? Assessment of the elastic modulus of the pancreas and comparison with tactile sensation, histology, and occurrence of postoperative pancreatic fistula after pancreaticoduodenectomy. Surgery. [In press].

[27] Kojima M, Shiokawa A, Ohike N, et al. Clinical significance of nuclear morphometry at the invasive front of T1 colorectal cancer and relation to expression of VEGF-A and VEGF-C. Oncology 2005;68:230.

[28] Tobin NP, Lundgren KL, Conway C, et al. Automated image analysis of cyclin D1 protein expression in invasive lobular breast carcinoma provides independent prognostic information. Hum Pathol 2012;43:2053.

[29] Aizawa M, Kojima M, Gotohda N, et al. Geminin expression in pancreatic neuroendocrine tumors: possible new marker of malignancy. Pancreas 2012;41:512.

[30] Ammann RW, Heitz PU, Klöppel G. Course of alcoholic chronic pancreatitis: a prospective clinicomorphological long-term study. Gastroenterology 1996;111:224.

[31] Rzepko R, Jaśkiewicz K, Klimkowska M, et al. Microvascular density in chronic pancreatitis and pancreatic ductal adenocarcinoma. Folia Histochem Cytobiol 2003;41:237.

[32] Kuehn R, Lelkes PI, Bloechle C, et al. Angiogenesis, angiogenic growth factors, and cell adhesion molecules are upregulated in chronic pancreatic diseases: angiogenesis in chronic pancreatitis and in pancreatic cancer. Pancreas 1999;18:96.
[33] Friess H, Malfertheiner P, Isenmann R, et al. The risk of pancreaticointestinal anastomosis can be predicted preoperatively. Pancreas 1996;13:202.
[34] Menahem B, Guittet L, Mulliri A, et al. Pancreaticogastrostomy is superior to pancreaticojejunostomy for prevention of pancreatic fistula after pancreaticoduodenectomy: an updated meta-analysis of randomized controlled trials. Ann Surg; 2014 Jun 27.
[35] Xiong JJ, Tan CL, Szatmary P, et al. Meta-analysis of pancreaticogastrostomy versus pancreaticojejunostomy after pancreaticoduodenectomy. Br J Surg 2014;101:1196.
[36] Allen PJ, Gönen M, Brennan MF, et al. Pasireotide for postoperative pancreatic fistula. N Engl J Med 2014;370: 2014.

Eur Radiol
DOI 10.1007/s00330-014-3558-2

INTERVENTIONAL

Retrograde-outflow percutaneous isolated hepatic perfusion using cisplatin: A pilot study on pharmacokinetics and feasibility

Satoru Murata · Shiro Onozawa · Takahiko Mine · Tatsuo Ueda · Fumie Sugihara · Daisuke Yasui · Shin-ichiro Kumita · Mitsuo Satake

Received: 24 May 2014 / Revised: 26 November 2014 / Accepted: 4 December 2014

Abstract
Objectives This study aimed to evaluate the feasibility and underlying pharmacokinetics of the retrograde-outflow technique for percutaneous isolated hepatic perfusion (PIHP).
Methods Retrograde-outflow PIHP was performed in 12 male pigs (weight, 37–44 kg) by redirecting hepatic outflow through the portal vein. Blood with cisplatin (2.5 mg/kg) in an extracorporeal circuit was circulated through the liver under isolation using rotary pumps with balloon catheters. Hepatic angiographic examinations were conducted during perfusion, and histopathological examinations of the organs were conducted after perfusion. The maximum platinum concentration (C_{max}), area under the concentration-time curve (AUC), and chronologic laboratory data were measured.
Results Retrograde-outflow isolated hepatic angiography confirmed that contrast media flowed into the portal veins in all 12 pigs. The hepatic veins and inferior vena cava were not opacified. Hepatic C_{max} (86.3 mg/l) was 39-fold greater than systemic C_{max} (2.2 mg/l), and hepatic AUC (1330.8 min·mg/l) was 30-fold greater than systemic AUC (44.6 min·mg/l). Histopathological examinations revealed no ischaemic changes or other abnormalities in the liver, duodenum, small intestine, or colon. Within 1 week of the procedure, chronologic laboratory data (n=3) normalized or returned to pre-therapy levels.
Conclusions The retrograde-outflow technique appears to enable safe and feasible PIHP therapy.

S. Murata (✉) · S. Onozawa · T. Mine · T. Ueda · F. Sugihara · D. Yasui · S.-i. Kumita
Department of Radiology/Center for Advanced Medical Technology, Nippon Medical School, 1-1-5 Sendagi, Bunkyou-ku, Tokyo, 113-8602, Japan
e-mail: genji@nms.ac.jp

M. Satake
Department of Diagnostic Radiology, National Cancer Center Hospital East, 6-5-1 Kashiwanoha Kashiwa, Chiba, 277-8577, Japan

Published online: 18 December 2014

Key Points
- *The portal vein acted as an outflow tract under retrograde-outflow PIHP.*
- *Plasma hepatic-to-systemic exposure ratio was 39.2 for the maximum platinum concentration.*
- *Plasma hepatic-to-systemic exposure ratio was 29.8 for the AUC.*
- *The retrograde-outflow technique appears to enable safe and feasible PIHP.*

Keywords Liver · Isolation perfusion cancer chemotherapy · Percutaneous · Retrograde · Experimental

Introduction

Several forms of locoregional treatment have been used to manage primary and secondary unresectable liver malignancies. Repeated transcatheter arterial infusion (TAI) therapy yields higher response rates than systemic chemotherapy; however, no convincing evidence of a long-term survival benefit has been found [1–4]. Transcatheter arterial chemoembolization (TACE), a widely used palliative treatment, is based on a high degree of tumour arterialization [5, 6]. However, the effectiveness of transcatheter treatment is reduced by the presence of dual blood supply (i.e., arterial and portal) to hepatic tumours, which makes it impossible to deliver anticancer agents to the entire tumour or to achieve sufficient tumour ischaemia without irreversibly damaging the surrounding non-tumorous parenchyma [7–9].

Several researchers have obtained promising results by using surgically isolated hepatic perfusion (IHP) to overcome this obstacle [10–13]. Isolated perfusion is a method to separate the hepatic circulation from the systemic circulation by occluding both hepatic inflow (the hepatic artery and portal vein) and outflow (hepatic vein), and connecting both to

extracorporeal pumps. Ligation and cannulation of each vessel is performed via laparotomy under IHP. However, this treatment is limited in that it requires an aggressive surgical intervention that is associated with considerable morbidity and mortality. Another limitation of this technique is that it does not allow for repeated intervention, mainly because of the formation of adhesions [10, 12–15]. Because laparotomy is unnecessary, percutaneous IHP techniques using balloon occlusion catheters may potentially result in lower procedural morbidity and shorter operative times. Furthermore, percutaneous IHP techniques with balloon occlusion catheters can enable repeated administration of chemotherapy in the same patient, potentially resulting in greater therapeutic efficacy in the treatment of unresectable liver tumours [16, 17]. IHP utilizes an orthograde approach, by employing the hepatic artery as an inflow route and the inferior vena cava (IVC) through the hepatic veins as an outflow route, similar to the physiologic condition. In previous studies, percutaneous IHP techniques showed higher rates of leakage from the perfusion circuit into the systemic circulation [16–19], mainly because the distance between the origins of the right atrium and the hepatic vein is often too short to allow balloon occlusion of the suprahepatic IVC without occluding the hepatic veins themselves [16, 19] and incompletely occluding the IVC or diaphragmatic veins. All orthograde IHP techniques that employ a double-balloon catheter for IVC occlusion, including combinations of orthograde percutaneous and surgical IHP techniques, may develop increased leakage into the systemic circulation because of this.

In acute segmental hepatic venous outflow occlusion, the corresponding liver parenchyma is supplied only by the artery and drained via the portal vein [20, 21], suggesting that retrograde IHP could be applied by employing hepatic artery inflow and portal vein outflow. Based on this theory, we developed a retrograde-outflow percutaneous IHP circulation system (R-PIHP) by redirecting hepatic outflow through the portal vein. The aim of this study was to evaluate the feasibility and the underlying pharmacokinetics of R-PIHP.

Materials and methods

Animal model

The Animal Experiment Ethics Committee of our university approved all animal experiments. Surgical procedures were performed under sterile conditions and anaesthesia, in 12 male pigs weighing 37–44 kg (mean, 42 kg). A veterinary physician was also involved in the study. The liver of each animal was shown to be morphologically normal by ultrasound examination prior to the procedure. The results of blood studies were within normal limits prior to the procedure.

Systemic circulation monitoring

Peripheral arterial oxygen saturation was maintained at > 95 % and was monitored using a probe that was applied to the ear. Each animal was monitored by electrocardiography throughout the procedures. The left axillary artery and left jugular vein were exposed through cut-down incisions, and a cannula sheath (5-French; Terumo Clinical Co., Ltd., Tokyo, Japan) was inserted into each vessel. The left axillary artery cannula was used to monitor blood pressure during the procedures. The left jugular vein cannula was used to collect blood samples and administer Ringer's solution (Lactec G injection; Otsuka Pharmaceutical Co. Ltd., Iwate, Japan) by intravenous drip infusion.

Catheterization and perfusion techniques

Figure 1 illustrates the techniques used for this study.

Construction of the isolated hepatic circuit

Infusion site: hepatic artery The right common femoral artery was exposed through cut-down incisions, and an 8-French cannula sheath (Medikit Co. Ltd., Tokyo, Japan) was inserted.

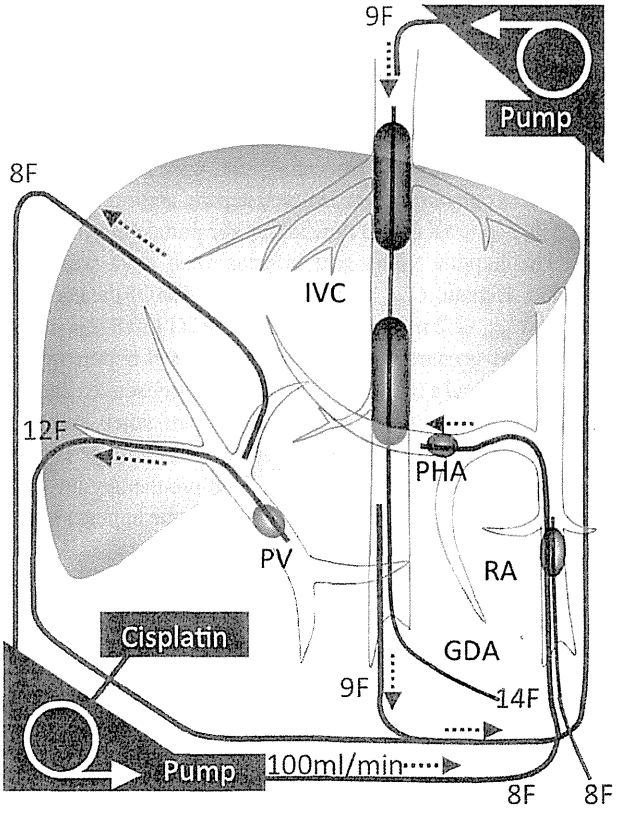

Fig. 1 The technique used for retrograde-outflow isolated hepatic perfusion. IVC, inferior vena cava; PV, portal vein; GDA, gastroduodenal artery; PHA, proper hepatic artery; RA, renal artery

Anterior mesenteric arteriography and celiac arteriography were performed for anatomical mapping. The gastroduodenal artery was embolized with coils to prevent drug leakage. The 8-French balloon catheter (Terumo Clinical Co., Ltd.) was then positioned in the common hepatic artery.

Aspiration site: portal vein Two intrahepatic portal branches were punctured with an 18-gauge percutaneous transhepatic cholangiography needle under ultrasonographic guidance. An 8-French cannula sheath with side holes was inserted into the portal vein to aspirate blood with cisplatin from the intrahepatic portal veins. A 12-French sheath was inserted into the portal vein. After systemic heparinization (120 U/kg), one 12-French cannula sheath with a 35-mm balloon (Forte Co., Ltd., Tokyo, Japan) was placed in the portal vein trunk to aspirate outflow blood via the anterior mesenteric and splenic veins (aspiration pressure at < 100 mm Hg) and return the blood into the jugular vein. This technique offered two advantages for R-PIHP. First, it compensated for decreased systemic venous return. Second, it prevented the inflow of blood via the anterior mesenteric and splenic veins into the intrahepatic portal veins beyond the portal occlusion balloon catheter.

Redirecting the hepatic outflow through the portal vein One 14-French double-balloon catheter with 35-mm balloons (Forte Co., Ltd.) was placed via the right femoral vein into the hepatic portion of the suprarenal vena cava to occlude the hepatic veins.

Perfusion technique The balloon catheters in the hepatic artery, abdominal aorta, portal vein, and IVC were inflated in that order. The abdominal aorta was occluded just below the renal artery to compensate for decreased systemic venous return [22], by using a balloon catheter with a 35-mm balloon (Forte Co., Ltd.) that was inserted via the left femoral artery. After confirming the patency of the R-PIHP system by isolated hepatic arteriography, blood containing cisplatin (Nippon Kayaku Co., Ltd., Tokyo, Japan) was injected into the hepatic artery (injection rate, 100 ml/min) while blood was aspirated from the portal vein (aspiration rate, 100 ml/min) using rotary pumps. The period of R-PIHP therapy was fixed at 30 min. The total liver ischaemia time never exceeded 45 min [16].

Construction of the systemic circuit

Prior to vessel occlusion at each site, blood from the anterior mesenteric and splenic veins was aspirated via the tip of the balloon occlusion catheter in the portal vein trunk by using a rotary pump, while maintaining aspiration pressure at < 100 mm Hg to avoid haemolysis. Another 9-French cannula sheath was inserted into the IVC via the left femoral vein for IVC blood aspiration at a pressure of < 100 mm Hg. The rotary pumps were started after vessel occlusion, and the aspirated blood from each site was returned to the right jugular vein.

Choice of drug and dosage

Many researchers have used alkylating agents, such as melphalan, for the treatment of various types of tumours in IHP [17]; however, melphalan has not been authorized for use in Japan. Therefore, we decided to use cisplatin as a reference drug. The use of a large range of cisplatin doses (from 0.5 mg/kg to 3 mg/kg) [23, 24] has been reported in previous studies on IHP therapies. In the present study, we chose a relatively high cisplatin dose of 2.5 mg/kg body weight, because melphalan content in tumour tissue has been shown to be unaffected with either orthograde or retrograde IHP, although melphalan content in the liver was reduced by 80 % using the retrograde technique [25]. Moreover, an in vivo fluorescent microscopic study in a rat tumour model demonstrated that blood flow in the major portion of the hepatic lobules was stopped during retrograde IHP, with enhancement of only 40.7 % of the liver parenchyma [26].

Measurements and assessments

Effects of R-PIHP on haemodynamics Haemodynamic parameters, arterial blood pressure, and heart rate were measured before, during, and after R-PIHP. None of the pigs received vasopressor agents.

Confirmation of the R-PIHP system Digital subtraction angiography was performed before R-PIHP therapy by the injection of contrast media (300 mg I/ml) into the hepatic artery to confirm the patency of the R-PIHP system. The rotary pumps achieved a perfusion rate of 100 ml/min with the same aspiration rate. Hepatic arteriography was performed using 30 ml of contrast media injected into the hepatic artery and then aspirated from the portal vein. Isolated hepatic arteriography was performed to verify that contrast media flowed only into the liver, with no extrahepatic opacification, and that the contrast media in the liver flowed into the intrahepatic portal vein, and not into the IVC.

Pharmacokinetics of the serum platinum concentration Plasma platinum concentrations were measured in blood samples collected from the hepatic arterial circulation and systemic venous circulation (superior vena cava) before and at 1, 3, 5, 10, 20, and 30 min after beginning R-PIHP. The maximum platinum concentration (C_{max}) and the area under the platinum blood concentration-time curve (AUC) were determined from these data and compared for each site. Plasma samples were digested with nitric acid for analysis of metal species. Platinum concentrations were measured using atomic

absorption spectrophotometry (Spectra AA-300/400 Zeeman; Varian Corp., Sydney, Australia).

Chronologic laboratory data after R-PIHP Three of the12 animals underwent embolization of the puncture routes using coils and gelatin sponges after the conclusion of R-PIHP therapy. These three animals were kept alive for one week for serial laboratory testing.

Vivisection and histological examinations Vivisection was performed immediately (n=9) and seven days (n=3) after R-PIHP therapy. The liver, duodenum, small intestine, and colon were removed by laparotomy in 12 pigs, and the spleen was removed in 3 pigs 7 days after R-PIHP. All pigs were sacrificed after organ removal by an intravenous injection of potassium chloride. Tissues were fixed in 10 % buffered formalin and embedded in paraffin for histological examination. Sections were stained with haematoxylin and eosin. Other stains were used, if necessary, at the discretion of an experienced pathologist.

Statistical analyses

All results are expressed as mean and 95 % confidence interval (95 % CI). All the parameters related to haemodynamic changes and the pharmacokinetics of cisplatin were analysed with paired t-tests. SPSS version 21 software (SPSS Japan, Inc., Tokyo, Japan) was used for all statistical analyses. Values of $P<0.05$ were considered statistically significant.

Results

Percutaneous R-PIHP was successfully performed in all pigs. The measurement of systemic and arterial platinum (infusion site) concentrations in the hepatic circulation was also successful in all cases.

Effects of R-PIHP on haemodynamics

The systolic arterial blood pressure decreased by 14 mm Hg (13.9 %) on average (range, 8–20 mm Hg, 7.1 – 19.6 %; $P<0.001$), within 3 min of balloon occlusion of the IVC. Blood pressure remained stable at this level during R-PIHP and recovered immediately after deflation of the IVC balloon ($P<0.001$). Heart rates remained stable before, during, and after R-PIHP therapy.

Confirmation of the R-PIHP system

Retrograde-outflow isolated hepatic arteriography with rotary pumps (Fig. 2) confirmed that contrast media flowed into both the liver and the intrahepatic portal vein. The absence of opacification of the hepatic veins and IVC was confirmed in all pigs. Contrast opacification of the main portal trunk increased with time, confirming that the portal vein acted as an outflow tract. No collateral vessels to the surrounding organs were opacified during arteriography. In summary, these results suggest complete occlusion of the IVC and portal vein and verified the patency of the R-PIHP system in all pigs.

Pharmacokinetics of the serum platinum concentration

The systemic and hepatic circulatory serum platinum concentrations were measured in all pigs (Table 1). The mean C_{max} in the hepatic circulation was 86.3 mg/l (95 % CI, 73.8 – 98.7 mg/l) and the mean AUC was 1,330.8 mg·min/l (95 % CI, 1,128.2 – 1,533.4 mg·min/l). In contrast, the mean C_{max} in the systemic circulation was 2.2 mg/l (95 % CI, 1.6 – 2.9 mg/l) and the mean AUC was 44.6 mg·min/l (95 % CI, 29.5 –

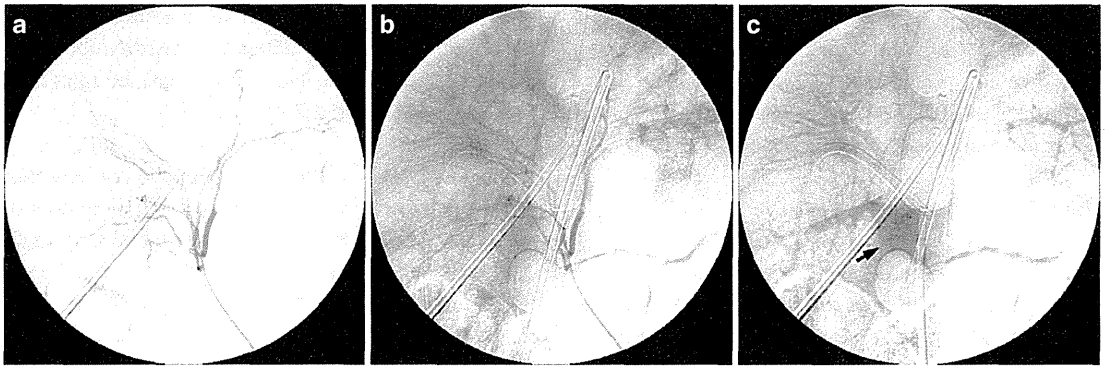

Fig. 2 Isolated hepatic angiography images obtained during the retrograde-outflow procedure. Contrast media flowed into the liver (A, early arterial phase; B, late arterial phase) and intrahepatic portal vein (C, portal phase). The hepatic veins and inferior vena cava were not opacified. Contrast opacification of the main portal trunk increased with time (C, arrow), confirming that the portal vein acted as an outflow tract. No collateral vessels to the surrounding organs were opacified

Table 1 C_{max} and AUC of platinum in the hepatic and systemic circulation

	HC		SC		HC/SC Exposure Ratio	
Pig	C_{max}	AUC	C_{max}	AUC	C_{max}	AUC
1	95.5	1500.7	1.1	13.6	85.3	110.5
2	78.5	1443.4	3.3	67.4	23.8	21.4
3	63.9	999.5	1.2	19.7	55.1	50.7
4	112.8	1802.1	2.0	37.7	57.3	47.8
5	51.8	1184.3	0.5	9.3	101.6	128.0
6	103.3	1305.2	3.3	81.9	30.9	15.9
7	92.6	863.5	2.0	44.3	47.0	19.5
8	105.2	1317.5	3.4	60.4	31.4	21.8
9	61.5	946.7	2.6	50.3	24.1	18.8
10	76.8	1450.8	1.5	24.5	50.5	59.3
11	90.4	1909.8	3.2	57.6	28.6	33.1
12	103.0	1246.5	2.8	68.6	37.1	18.2
Mean	86.3	1330.8	2.2	44.6	39.2	29.8
95% CI	73.8–98.7	1128.2–1533.4	1.6–2.9	29.5–59.7	32.1–63.3	21.5–69.3

The C_{max} is represented in mg/l, and the AUC for minutes 0–30 is indicated in mg·min/l.

C_{max} maximum platinum concentration,, *AUC* area under the concentration–time curve,, *CI* confidence interval,, *HC* hepatic circulation,, *SC* systemic circulation

59.7 mg·min/l). Platinum concentrations in the hepatic circulation were significantly higher ($P<0.01$) than those in the systemic circulation in all cases (Fig. 3). The hepatic-to-systemic circulation exposure ratio was 39.2 for C_{max} and 29.8 for the AUC.

Laboratory data

The laboratory data ($n=3$) are shown in Table 2 and Fig. 4. The levels of total protein, albumin, total bilirubin, and creatinine were within the normal range or were unchanged for one week after the procedure. Amylase, creatine phosphokinase (CK), aspartate aminotransferase (AST), alanine aminotransferase (ALT), and lactate dehydrogenase (LDH) levels were increased after R-PIHP therapy. Each value peaked in one or three days after therapy, and then decreased with time until returning to the normal range or pre-therapy levels.

Vivisection and histological examinations

The liver, duodenum, small intestine, colon, and spleen had a normal appearance in all cases. No vascular obstruction, stenosis, or haemorrhage was observed in the liver or abdominal aorta. Histological assessment revealed no evidence of structural disorder, sinusoidal dilatation, or thrombi in the hepatic vessels. None of the examined organs in any of the pigs showed ischaemic or oedematous changes. No significant effect was observed in the liver parenchyma, or any other organs, due to the administration of cisplatin.

Discussion

Animal studies of IHP have demonstrated that this technique delivers intrahepatic concentrations of cytostatic agents that are up to five-fold higher than those delivered by TAI [27, 28].

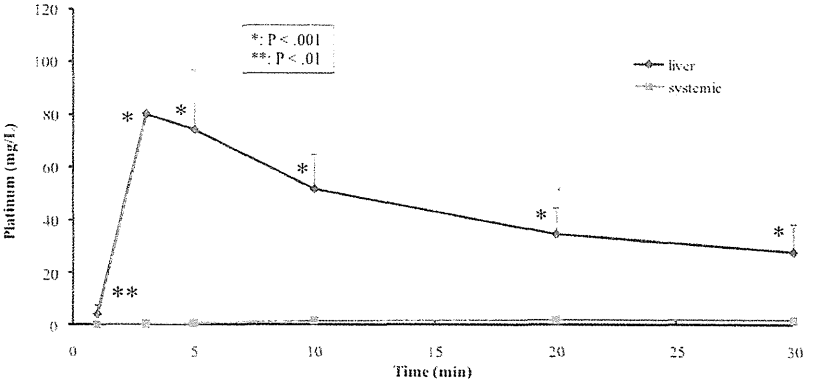

Fig. 3 Serum plasma platinum concentrations during retrograde-outflow isolated hepatic perfusion. All platinum concentrations in the hepatic circulation were significantly higher ($P<0.01$, paired t-test) than those in the systemic circulation.

Table 2 Chronologic laboratory data before and after the procedure

	Normal range	Pre-procedure	Post-procedure	1 day after	3 days after	5 days after	7 days after
TP	5.8–9.1 (g/dl)	5.1 (4.3, 6.0)	4.5 (2.7, 6.3)	5.8 (4.4, 7.2)	6.1 (5.0, 7.1)	6.1 (4.9, 7.4)	6.1 (4.7, 7.5)
Alb	3.2–4.8 (g/dl)	2.8 (2.6, 3.0)	2.5 (2.1, 2.8)	3.1 (2.3, 3.9)	3.2 (2.4, 3.9)	3.2 (2.0, 4.5)	3.1 (1.9, 4.4)
T-Bil	< 0.5 (mg/dl)	0.1 (0.0, 0.3)	0.1 (0.0, 0.3)	0.0 (0.0, 0.1)	0.0 (0.0, 0.1)	0.1 (0.0, 0.3)	0.0 (0.0, 0.1)
Cre	1.2–2.4 (mg/dl)	0.9 (0.3, 1.4)	1.1 (0.4, 1.8)	0.8 (0.7, 0.9)	0.9 (0.5, 1.3)	1.0 (0.6, 1.4)	1.0 (0.7, 1.3)
Amy	525–2105 (U/l)	1273.3 (390.7, 2155.9)	1398.3 (740.1, 2056.6)	2140.0 (1406.9, 2873.1)	1963.3 (521.0, 3405.6)	1731.0 (427.9, 3034.1)	1666.0 (492.1, 2839.9)
CK	679–3161 (U/l)	750.0 (453.1, 1046.9)	1281.0 (410.6, 2151.4)	1941.0 (1583.7, 2298.3)	4233.3 (1422.6, 7044.1)	1166.3 (199.4, 2133.3)	927.7 (14.6, 1840.8)
AST	< 44 (U/l)	26.7 (3.6, 49.7)	61.3 (15.4, 107.3)	95.3 (31.9, 158.8)	85.3 (13.9, 156.7)	44.7 (0.0, 99.2)	19.0 (0.2, 37.8)
ALT	< 58 (U/l)	29.3 (10.7, 48.0)	31.3 (5.2, 57.4)	73.3 (0.0, 171.2)	62.3 (37.0, 87.7)	47.7 (41.4, 53.9)	38.7 (15.6, 61.7)
LDH	577–1525 (U/l)	346.7 (268.0, 425.3)	399.0 (346.4, 451.6)	1111.0 (0.0, 3156.9)	986.3 (0.0, 2151.4)	736.7 (0.0, 1586.5)	520.0 (0.0, 1061.6)

Data in parentheses are 95% CIs.

TP total protein, *Alb* albumin, *T-Bil* total bilirubin, *Cre* creatinine, *Amy* amylase, *CK* creatine phosphokinase, *AST* aspartate aminotransferase, *ALT* alanine aminotransferase, *LDH* lactate dehydrogenase

IHP also makes it possible to use perfusion drugs that do not have a high first-pass hepatic extraction rate, facilitating the prolonged exposure of the tumour to these drugs without concomitant systemic exposure. This advantage of IHP over TAI has yielded encouraging results in terms of prolonged survival in patients with metastatic liver tumours [10–13]. The use of anticancer drugs that demonstrate high systemic toxicity, such as tumour necrosis factor, might therefore become possible because the liver vascular bed can be cleared after perfusion. However, a feasible protocol for safe and repeatable percutaneous IHP is very desirable due to the associated major surgical trauma, morbidity, and the inability to repeat surgical IHP [10, 12–15].

The current orthograde percutaneous IHP techniques have been associated with significant leakage into the systemic circulation in clinical situations [16, 17, 29], contrary to results obtained in experimental settings [22]. The major reason is that the human suprahepatic vena cava is shorter than that of the pig, rendering its occlusion with a balloon difficult [19] and resulting in incomplete occlusion of the IVC or diaphragmatic veins. However, the IVC and some diaphragmatic veins can be occluded by clamping during an open surgical procedure without obstruction of the hepatic veins. In the present study, by using the R-PIHP technique, which allows outflow via the portal vein, we were able to overcome the anatomical disadvantage of the short human suprahepatic vena cava and

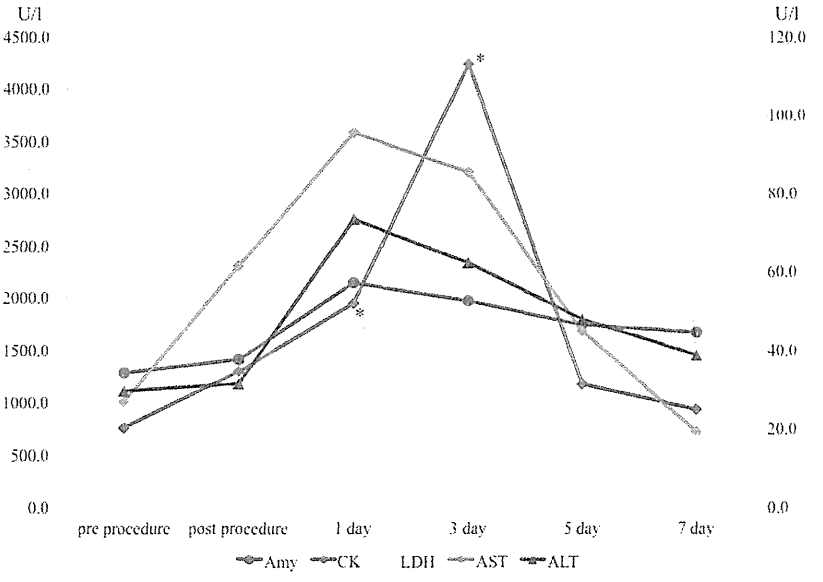

Fig. 4 Chronologic laboratory data before and after the procedure. Amylase, creatine kinase (CK), aspartate aminotransferase (AST), alanine aminotransferase (ALT), and lactate dehydrogenase (LDH) levels increased after retrograde-outflow percutaneous isolated hepatic perfusion therapy. Each value peaked one or three days after therapy and then decreased until they returned to normal or pre-therapy values. *: $P<0.05$; Repeated analysis of variance and post-hoc analysis between the pre-procedural values and each measurement

the accompanying disadvantage of leakage via the IVC and diaphragmatic veins. The underlying principle is that occlusion of the IVC at the hepatic portion including the diaphragmatic veins provides an alternative to normal hepatic circulation [20, 21]. In the present study, isolated hepatic angiography clearly showed reversal of blood flow from the liver parenchyma into the portal vein, indicating the conversion of the portal vein from an inflow to an outflow vessel. This phenomenon occurs because of the high pressure generated in the periportal sinusoids by the continuous flow of blood draining into the sinusoids via the peribiliary plexus [26, 30]. The high pressure from the peribiliary plexus forces blood from the remaining sinusoids and hepatic veins to drain toward the lower pressure portal vein.

The pharmacokinetic data further demonstrated that R-PIHP is not inferior to orthograde percutaneous techniques or combined orthograde and surgical percutaneous IHP used in experimental pig studies [22]. In this context, it is relevant to consider whether percutaneous R-PIHP is a safe, efficacious, and feasible alternative to surgical IHP for hepatic malignancies. Although direct comparisons of this experimental study and previous clinical studies may not be precise, slightly more systemic leakage was observed in the present study compared with previously published orthograde surgical IHP methods. Surgical IHP has a low systemic leakage rate of approximately 3 % [19, 31–33] and a very high hepatic-to-systemic AUC ratio of 52.0 [32]. However, the hepatic-to-systemic circulation exposure ratio in 42 % (5/12) of the pigs in the present study was similar to that of other surgical IHP methods in terms of systemic leakage. These pharmacokinetic differences may be due to the techniques and instruments used, and further technical refinements may overcome this disadvantage of the R-PIHP system.

With regard to the safety of percutaneous procedures, the most common side effect has been transient hypotension, secondary to the reduction of venous return to the heart as a result of IVC occlusion [18]. Vasoactive cardiotropic agents are usually administered to maintain haemodynamic stability when the balloons are inflated, as venous return is compromised [18, 34]. In the present study, the aorta was occluded with a balloon just below the renal artery [22] to compensate for the decreased systemic venous return, creating a haemodynamically acceptable IHP system. Laboratory data showed a transient increase in values after R-PIHP therapy, but an eventual return to normal or pre-therapy levels. Histological assessment also revealed no evidence of abnormal findings in any of the pigs. Therefore, the R-PIHP technique appears to be a safe percutaneous approach to IHP therapy.

There were two main limitations to the present study. First, we used cisplatin as a reference drug; therefore, we could not directly compare drug leakage between the present study and previous studies that used alkylating agents such as melphalan, which is unavailable in Japan. Second, we did not use a tumour model because no such pig liver tumour model currently exists. Therefore, the efficacy of R-PIHP therapy was not confirmed. This was a pilot study that was designed to study the feasibility, pharmacokinetics, and potential benefits of R-PIHP.

In conclusion, our R-PIHP technique, wherein inflow was achieved via the hepatic artery and outflow was achieved via the portal vein, appears to be a feasible and safe percutaneous approach to IHP therapy.

Acknowledgements The scientific guarantor of this publication is Satoru Murata. The authors of this manuscript declare no relationships with any companies whose products or services may be related to the subject matter of the article. This study has received funding by grants from the Third Term Comprehensive Control Research for Cancer, the Program for Promotion of Fundamental Studies in Health Sciences of the Organization for Pharmaceuticals and Medical Devices Agency (PMDA) of the Ministry of Health, Labor and Welfare, and the Grant-in-Aid for Scientific Research (S and B) from the Ministry of Education, Culture, Sports, Science and Technology, Japan. No complex statistical methods were necessary for this paper. Institutional Review Board approval was not required because this was an experimental animal study. Written informed consent was not required for this study because this was an experimental animal study. Approval from the institutional animal care committee was obtained. Some study subjects or cohorts have not been previously reported. Methodology: prospective, experimental, performed at one institution.

References

1. Yoon SS, Tanabe KK (1999) Surgical treatment and other regional treatments for colorectal cancer liver metastases. Oncologist 4:197–208
2. Kemeny N, Fata F (2001) Hepatic-arterial chemotherapy. Lancet Oncol 2:418–428
3. Nouso K, Miyahara K, Uchida D et al (2013) Effect of hepatic arterial infusion chemotherapy of 5-fluorouracil and cisplatin for advanced hepatocellular carcinoma in the Nationwide Survey of Primary Liver Cancer in Japan. Br J Cancer 109:1904–1907
4. Tsai WL, Lai KH, Liang HL et al (2014) Hepatic Arterial Infusion Chemotherapy for Patients with Huge Unresectable Hepatocellular Carcinoma. Plos One. doi:10.1371/journal.pone.0092784
5. Yamada R, Sato M, Kawabata M, Nakatsuka H, Nakamura K, Takashima S (1983) Hepatic artery embolization in 120 patients with unresectable hepatoma. Radiology 148:397–401
6. Uchida H, Matsuo N, Sakaguchi H, Nagano N, Nishimine K, Ohishi H (1993) Segmental embolotherapy for hepatic cancer: keys to success. Cardiovasc Interv Radiol 16:67–71
7. Ackerman BN (1972) Experimental studies on the circulatory dynamics of intrahepatic tumor blood supply. Cancer 29:435–439
8. Kan Z, Ivancev K, Lunderquist A et al (1993) In vivo microscopy of hepatic tumors in animal models: a dynamic investigation of blood supply to hepatic metastases. Radiology 187:621–626
9. Kan Z, Wallace S (1997) Transcatheter liver lobar ablation: an experimental trial in an animal model. Eur Radiol 7:1071–1075
10. Vahrmeijer AL, van Dierendonck JH, Keizer HJ et al (2000) Increased local cytostatic drug exposure by isolated hepatic perfusion: a phase I clinical and pharmacologic evaluation of treatment with high dose melphalan in patients with colorectal cancer confined to the liver. Br J Cancer 82:1539–1546

11. Christoforidis D, Martinet O, Lejeune FJ, Mosimann F (2002) Isolated liver perfusion for non-resectable liver tumours: a review. Eur J Surg Oncol 28:875–890
12. Rothbarth J, Pijl ME, Vahrmeijer AL et al (2003) Isolated hepatic perfusion with high-dose melphalan for the treatment of colorectal metastasis confined to the liver. Br J Surg 90:1391–1397
13. Alexander HR Jr, Bartlett DL, Libutti SK et al (2009) Analysis of factors associated with outcome in patients undergoing isolated hepatic perfusion for unresectable liver metastases from colorectal cancer. Ann Surg Oncol 16:1852–1859
14. van Iersel LB, Gelderblom H, Vahrmeijer AL et al (2008) Isolated hepatic melphalan perfusion of colorectal liver metastases: outcome and prognostic factors in 154 patients. Ann Oncol 19:1127–1134
15. Zeh HJ III, Brown CK, Holtzman MP et al (2009) A phase I study of hyperthermic isolated hepatic perfusion with oxaliplatin in the treatment of unresectable liver metastases from colorectal cancer. Ann Surg Oncol 16:385–394
16. Savier E, Azoulay D, Huguet E, Lokiec F, Gil-Delgado M, Bismuth H (2003) Percutaneous isolated hepatic perfusion for chemotherapy: a phase 1 study. Arch Surg 138:325–332
17. Pingpank JF, Libutti SK, Chang R et al (2005) Phase I study of hepatic arterial melphalan infusion and hepatic venous hemofiltration using percutaneously placed catheters in patients with unresectable hepatic malignancies. J Clin Oncol 23:3465–3474
18. Ravikumar TS, Pizzorno G, Bodden W et al (1994) Percutaneous hepatic vein isolation and high-dose hepatic arterial infusion chemotherapy for unresectable liver tumors. J Clin Oncol 12:2723–2736
19. Rothbarth J, Tollenaar RA, Schellens JH et al (2004) Isolated hepatic perfusion for the treatment of colorectal metastases confined to the liver: recent trends and perspectives. Eur J Cancer 40:1812–1824
20. Murata S, Itai Y, Asato M et al (1995) Effect of temporary occlusion of hepatic vein on dual blood supply in the liver: evaluation with spiral CT. Radiology 197:351–356
21. Murata S, Itai Y, Satake M et al (1997) Changes in contrast enhancement of hepatocellular carcinoma and liver: effect of temporary occlusion of a hepatic vein evaluated with spiral CT. Radiology 202:715–720
22. van Ijken MG, de Bruijn EA, de Boeck G, ten Hagen TL, van der Sijp JR, Eggermont AM (1998) Isolated hypoxic hepatic perfusion with tumor necrosis factor-α, melphalan, and mitomycin C using balloon catheter techniques a pharmacokinetic study in pigs. Ann Surg 228: 763–770
23. Hafström LR, Holmberg SB, Naredi PL et al (1994) Isolated hyperthermic liver perfusion with chemotherapy for liver malignancy. Surg Oncol 3:103–108
24. Ortega-Deballon P, Facy O, Consolo D et al (2010) Hypoxic single-pass isolated hepatic perfusion of hypotonic cisplatin: Safety study in the pig. Ann Surg Oncol 17:898–906
25. Rothbarth J, Sparidans RW, Beijnen JH et al (2002) Reduced liver uptake of arterially infused melphalan during retrograde rat liver perfusion with unaffected liver tumour uptake. J Pharmacol Exp Ther 303:736–740
26. Murata S, Jeppsson B, Lunderquist A, Ivancev K (2014) Hemodynamics in rat liver tumor model during retrograde-outflow isolated hepatic perfusion with aspiration from the portal vein: angiography and in vivo microscopy. Acta Radiol 55:737–744
27. Marinelli A, van de Velde CJ, Kuppen PJ et al (1990) A comparative study of isolated liver perfusion versus hepatic artery infusion with mitomycin C in rats. Br J Cancer 62:891–896
28. Marinelli A, van Dierendonck JH, van Brakel GM et al (1991) Increasing the effective concentration of melphalan in experimental rat liver tumours: comparison of isolated liver perfusion and hepatic artery infusion. Br J Cancer 64:1069–1075
29. van Etten B, Brunstein F, van Ijken MG et al (2004) Isolated hypoxic hepatic perfusion with orthograde or retrograde flow in patients with irresectable liver metastases using percutaneous balloon catheter techniques: a phase I and II study. Ann Surg Oncol 11:598–605
30. Kan Z, Ivanchev K, Lunderquist A (1994) Peribiliary plexa—important pathways for shunting of iodized oil and silicon rubber solution from the hepatic artery to the portal vein: an experimental study in rats. Invest Radiol 29:671–676
31. Pilati P, Mocellin S, Rossi CR et al (2004) True versus mild hyperthermia during isolated hepatic perfusion: effects on melphalan pharmacokinetics and liver function. World J Surg 28:775–781
32. Mocellin S, Pilati P, Da Pian P et al (2007) Correlation between melphalan pharmacokinetics and hepatic toxicity following hyperthermic isolated liver perfusion for unresectable metastatic disease. Ann Surg Oncol 14:802–809
33. van Iersel LB, Veriaan MR, Vahrmeijer AL et al (2007) Hepatic artery infusion of high-dose melphalan at reduced flow during isolated hepatic perfusion for the treatment of colorectal metastases confined to the liver: a clinical and pharmacologic evaluation. Eur J Surg Oncol 33:874–881
34. Beheshti MV, Denny DF Jr, Glickman MG et al (1992) Percutaneous isolated liver perfusion for treatment of hepatic malignancy: preliminary report. J Vasc Interv Radiol 3:453–458

PLOS | ONE

RESEARCH ARTICLE

MicroRNA Markers for the Diagnosis of Pancreatic and Biliary-Tract Cancers

Motohiro Kojima[1]*, Hiroko Sudo[2], Junpei Kawauchi[2], Satoko Takizawa[2], Satoshi Kondou[3], Hitoshi Nobumasa[3], Atsushi Ochiai[1]

1 Department of Pathology, National Cancer Center Hospital East, Kashiwa, Chiba, Japan, **2** New Frontiers Research Laboratories, Toray Industries, Inc., Kamakura, Kanagawa, Japan, **3** New Projects Development Division, Toray Industries, Inc., Kamakura, Kanagawa, Japan

* mokojima@east.ncc.go.jp

OPEN ACCESS

Citation: Kojima M, Sudo H, Kawauchi J, Takizawa S, Kondou S, Nobumasa H, et al. (2015) MicroRNA Markers for the Diagnosis of Pancreatic and Biliary-Tract Cancers. PLoS ONE 10(2): e0118220. doi:10.1371/journal.pone.0118220

Academic Editor: Ajay Goel, Baylor University Medical Center, UNITED STATES

Received: July 24, 2014

Accepted: January 11, 2015

Published: February 23, 2015

Data Availability Statement: All microarray data from this study are in agreement with the Minimum Information About a Microarray Experiment (MIAME) and are publicly available through the Gene Expression Omnibus (GEO) database (http://www.ncbi.nlm.nih.gov/projects/geo/) under the accession number GSE59856.

Funding: HS, JK, ST, SK and HN were full-time employees of Toray Industries, Inc. at the time of the study. There are no constraints from the sponsors on use or dissemination of the data, or influence on the results or conclusions. The sponsors had no role in

Abstract

It is difficult to detect pancreatic cancer or biliary-tract cancer at an early stage using current diagnostic technology. Utilizing microRNA (miRNA) markers that are stably present in peripheral blood, we aimed to identify pancreatic and biliary-tract cancers in patients. With "3D-Gene", a highly sensitive microarray, we examined comprehensive miRNA expression profiles in 571 serum samples obtained from healthy patients, patients with pancreatic, biliary-tract, or other digestive cancers, and patients with non-malignant abnormalities in the pancreas or biliary tract. The samples were randomly divided into training and test cohorts, and candidate miRNA markers were independently evaluated. We found 81 miRNAs for pancreatic cancer and 66 miRNAs for biliary-tract cancer that showed statistically different expression compared with healthy controls. Among those markers, 55 miRNAs were common in both the pancreatic and biliary-tract cancer samples. The previously reported miR-125a-3p was one of the common markers; however, it was also expressed in other types of digestive-tract cancers, suggesting that it is not specific to cancer types. In order to discriminate the pancreato-biliary cancers from all other clinical conditions including the healthy controls, non-malignant abnormalities, and other types of cancers, we developed a diagnostic index using expression profiles of the 10 most significant miRNAs. A combination of eight miRNAs (miR-6075, miR-4294, miR-6880-5p, miR-6799-5p, miR-125a-3p, miR-4530, miR-6836-3p, and miR-4476) achieved a sensitivity, specificity, accuracy and AUC of 80.3%, 97.6%, 91.6% and 0.953, respectively. In contrast, CA19-9 and CEA gave sensitivities of 65.6% and 40.0%, specificities of 92.9% and 88.6%, and accuracies of 82.1% and 71.8%, respectively, in the same test cohort. This diagnostic index identified 18/21 operable pancreatic cancers and 38/48 operable biliary-tract cancers in the entire cohort. Our results suggest that the assessment of these miRNA markers is clinically valuable to identify patients with pancreato-biliary cancers who could benefit from surgical intervention.

study design, data collection and analysis, decision to publish, or preparation of the manuscript.

Competing Interests: At the time of the study, HS, JK, ST, SK and HN were full-time employees of Toray Industries, Inc. who provides marketed microarray products that were investigated in this study. However, this does not alter the authors' adherence to all the PLOS ONE policies on sharing data and materials.

Introduction

Pancreatic cancer is one of the most lethal cancers. Most pancreatic cancers do not accompany any particular clinical symptoms in the early stage, permitting the cancers to progress undetected. In addition, ambiguous radiological images of cancerous lesions and inflammatory conditions in the pancreas prevent pancreatic cancers from being correctly identified. Furthermore, the anatomical location of the pancreas, deep in a retroperitoneal space surrounded by many other organs, hinders the acquisition of a biopsy. All of these factors prevent the early detection of pancreatic cancer. The American Cancer Association estimated that 40,000 people would die of pancreatic cancer in 2014 in the United States [1]. The five-year survival rate for patients with exocrine pancreatic cancer is estimated at 14% for stage IA, but it drops to 1% for stage IV [1]. Because the most promising treatment for pancreatic cancer is surgical resection, detecting pancreatic cancer at surgically resectable stages is crucial for improving the survival rate of patients with pancreatic cancer. From this point of view, the screening of the early stages of pancreatic or biliary-tract cancers is imperative.

As a diagnostic screening method for pancreatic cancer, ultrasound is one of the most prevalent tests performed. However, this image analysis has its difficulty in differentiating non-malignant tissue from malignant tissue [2]. In addition, many tumor-associated antigens have been studied in connection with pancreatic cancer. The most validated and clinically useful biomarker is carbohydrate antigen (CA) 19–9; however, CA19-9 is known to be up-regulated in other inflammatory conditions, and its low positive predictive value makes it a poor biomarker for screening, limiting its current use mostly to the post-surgical monitoring of progressed pancreatic cancers [3, 4]. Today, there is no effective method to detect early, surgically resectable pancreatic cancers with sufficient diagnostic accuracy.

Recently, microRNAs (miRNAs) have been reported as potential biomarkers for various types of cancers. Using plasma samples from 50 cancer patients and ten healthy control subjects, as well as chemo-resistant pancreatic cell lines, Ali *et al.* suggested that serum miR-21 and other miRNAs could predict the aggressiveness of pancreatic cancer [5]. Ganepola *et al.* examined a dozen of plasma samples each from patients with and without pancreatic cancer, and concluded that three miRNAs, miR-642b, miR-885-5p, and miR-22, were more than 90% sensitive and specific in the diagnosis of pancreatic cancer [6]. Similarly, Li's group examined 20 or less serum samples each from patients with pancreatic cancer and control, respectively, as the biomarker discovery cohort, and found that multiple miRNAs including miR-1290 were useful in the early detection of pancreatic cancer [7]. More recently, researchers have analyzed more than 100 blood samples each from pancreatic cancer patients and controls, and some found miR-155, miR-181a, miR-181b and miR-196a [8], and others found miR-20a, miR-21, miR-24, miR-25, miR-99a, miR-185, and miR-191 [9] for blood miRNA markers. It should be noted that each of the previous studies suggested different circulating miRNA markers for pancreatic cancer. The discrepancies of previous studies could be attributed to various empirical factors that include the blood sample types (PBMC, plasma or serum), different detection technologies (PCR, microarray or sequencer), and heterogeneity of the sample cohorts. Especially, the sufficient size and the diversity of the sample cohorts are critical in biomarker research not only for the targeted group but also for the control group.

Here, we examined the expression profiles of comprehensive serum miRNAs from the largest cohorts of patients ever attempted: 100 patients with pancreatic cancer, 98 patients with biliary-tract cancer, 150 healthy control patients, 21 patients with non-malignant abnormalities in the pancreas or biliary tract, and 202 patients with other types of cancers. A highly sensitive microarray permitted the simultaneous analysis of more than 2,500 miRNAs that were recently updated in the miRBase (release 20), and serum samples from patients with the various clinical